Au-covered hollow urchin-like ZnO nanostructures for surface-enhanced Raman scattering sensing

Octavio Graniel, Igor Iatsunskyi, Emerson Coy, Christophe Humbert, Grégory Barbillon, Thierry Michel, David Maurin, Sébastien Balme, Philippe Miele, Mikhael Bechelany

Au-covered hollow urchin-like ZnO nanostructures for surface-enhanced Raman scattering sensing

Octavio Graniel[1], Igor Iatsunskyi[2], Emerson Coy[2], Christophe Humbert[3], Grégory Barbillon[4], Michel Thierry[5], David Maurin[5], Sébastien Balme[1], Philippe Miele[1,6], and Mikhael Bechelany*[1]

[1]Institut Européen des Membranes (IEM), UMR-5635, Université de Montpellier, ENSCM, CNRS, Place Eugène Bataillon, 34095 Montpellier, France

[2]NanoBioMedical Centre, Adam Mickiewicz University, 3 Wszechnicy Piastowskiej str., 61-614, Poznan, Poland

[3] Univ. Paris Sud, Université Paris Saclay, Laboratoire de Chimie Physique, CNRS, Bâtiment 201 P2, 91405 Orsay, France

[4]EPF-Ecole d'Ingénieurs, 3 bis rue Lakanal, 92330 Sceaux, France

[5]Laboratoire Charles Coulomb (L2C), Université de Montpellier, CNRS, Montpellier, France

[6]Institut Universitaire de France (IUF), MESRI, 1 rue Descartes, 75231 Paris, France

*** Corresponding author: mikhael.bechelany@umontpellier.fr**

Abstract

Au-covered hollow urchin-like ZnO nanostructures were prepared with controlled size by combining nanosphere lithography (NSL), atomic layer deposition (ALD), electrodeposition, and electron beam (e-beam) evaporation. The optimal Au film thickness was determined by measuring the surface-enhanced Raman scattering (SERS) intensities of the substrates. Furthermore, the sensing performances of these hybrid nanostructures have been investigated by using chemical and biological molecules: thiophenol and adenine, respectively. Limits of detection (LOD) of 10^{-8} M and 10^{-6} M were found for the detection of thiophenol and adenine, respectively. Additionally, the excellent uniformity and batch-to-batch reproducibility of the substrates make them excellent candidates for reliable SERS sensing and biosensing.

Highlights:

- Fabrication of Au-covered ZnO urchin-like structures for SERS sensing via high throughput methods
- SERS signal is homogenous throughout the substrate and reproducible by testing different batches
- The hybrid nanostructures offer promising prospects for the detection of adenine

Keywords: surface-enhanced Raman scattering, SERS substrates, atomic layer deposition, urchin-like ZnO, ZnO/Au heterostructure

Graphical abstract:

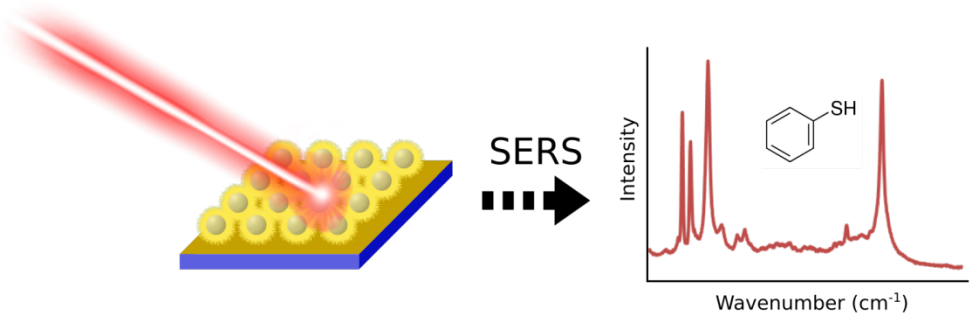

1. Introduction

Surface-enhanced Raman scattering (SERS) has emerged as one of the most powerful analytical techniques that offer single-molecule detection [1]. Its outstanding sensitivity and non-destructive character have found many applications in many fields such as chemistry [2], medicine [3], biology [4], and environmental sciences [5]. SERS substrates are mainly fabricated with noble metals (Ag, Au, Cu) due to their strong interaction with electromagnetic waves and the excitation of the localized surface plasmon resonance (LSPR) that can be tuned in the UV-Vis-NIR region [6,7]. These noble metals are usually combined with nanostructures such as nanospheres [8], nanowires [9], nanogaps [10], nanotrees [11], and nanorods [12] that provide roughened metal surfaces and plasmonically active "hotspots" that enhance the Raman signal by several orders of magnitude [13]. Additionally, thanks to their inherent SERS activity [14], semiconductors have been used to fabricate metal/semiconductor hybrid nanostructures that exhibit both electromagnetic enhancement and charge-transfer effects [12]. Furthermore, these highly-efficient SERS hybrids present additional properties that make them attractive for applications such as photocatalysis [15], water splitting [16], and solar energy conversion [17]. As a semiconductor material with a wide direct bandgap (3.37 eV), biocompatibility [18], and promising optoelectronic properties [19,20], ZnO has been employed for the construction of high-surface-area SERS substrates with a wide range of tunable morphologies [21].

However, the fabrication of reproducible and stable SERS substrates remains a major challenge [22]. Therefore, much attention has been paid to find facile, repeatable, and high-throughput fabrication methods for large-area nanostructured substrates. Among these methods, nanosphere lithography (NSL) has proven to be a reproducible and inexpensive technique that offers well-ordered arrays of nanostructures with wafer-scale throughput [23,24]. Thus, NSL has been used in combination with other techniques to fabricate different types of SERS substrates such as silver film over nanosphere (AgFON) [25], gold semishells [26], nanoring cavities [27], nanopyramids [28], and optrodes [29]. Recently, high-surface-area urchin-like structures decorated with Ag have been successfully used as SERS substrates [30–32]. Nevertheless, even though Ag is preferred over Au due to its higher SERS activity, Ag is prone to oxidation in air or water environments [33]. Consequently, decreasing its SERS enhancement factor (EF) as a result of changes in its chemical and plasmonic properties [34].

Herein, we report on a high-surface-area reproducible SERS substrate consisting of Au-covered ZnO urchin-like hollow structures for the detection of thiophenol. This substrate was fabricated by using

scalable techniques that include NSL, atomic layer deposition (ALD) [35], electrodeposition, and electron beam (e-beam) evaporation. NSL was used to obtain a template of well-organized spheres that were later covered with a seed layer of ZnO deposited by ALD. Afterward, ZnO nanowires (NWs) were grown via a hydrothermal method to obtain the urchin-like structures, which were finally subjected to e-beam evaporation of Au. Furthermore, we investigated the SERS performances of these hybrid nanostructures by detecting a small chemical molecule (thiophenol) and then a biomolecule (adenine).

2. Material and methods

2.1 Materials

Polystyrene (PS) spheres (aqueous dispersion, 10 % w/w) with a diameter of ~500 nm and sodium dodecyl sulfate (SDS, CAS: 151-21-3, purity > 99%) were purchased from Sigma-Aldrich and used as received. Zinc chloride (CAS: 7646-85-7, purity > 98%) and potassium chloride (CAS: 7447-40-7, purity > 99.0%) were purchased from Fluka. Thiophenol (CAS: 108-98-5, purity > 99%) was purchased from Alfa Aesar. Diethylzinc (DEZ, CAS: 557-20-0, purity > 95%) was purchased from Strem Chemicals Indium tin oxide (ITO) deposited on quartz was purchased from Präzisions Glas & Optik.

2.2 Fabrication of urchin-like ZnO structures covered by Au

First, ITO substrates (1 x 2 cm^2) were cleaned by sonication for 15 min in acetone, ethanol, and isopropanol sequentially and finally dried under air. After, the PS spheres were deposited on the ITO substrates using a previously reported method with slight modifications [36]. Briefly, a 1:2 solution of PS spheres and anhydrous ethanol was added dropwise with a micropipette onto the surface of a tilted glass slide (previously treated with oxygen plasma) that was resting on the wall of a Petri dish filled with deionized (DI) water. Afterwards, 5 µL of an SDS solution (10 wt. %) were added to the water surface to change the surface tension and pack together the PS spheres. The self-assembled PS spheres were then transferred to the ITO substrate (previously exposed to a 4 W, 254 nm UV lamp for 15 min to render it hydrophilic) by carefully introducing the substrate into the Petri dish and removing it from the solution at an angle of 45°. Once dry, the substrates were heated in an oven at 100 °C for 30 min to promote the adhesion of the PS spheres to the substrate. Next, the size of the spheres was reduced to produce a non–close-packed arrangement by reactive ion etching in O_2 plasma (0.6 mbar, 50W). The size of the PS spheres was controlled by adjusting the oxygen plasma exposure time.

Afterward, a 20-nm thick ZnO layer was deposited on the PS spheres-covered substrates by ALD in a home-made system. The ZnO films were grown at 80°C using diethyl zinc (DEZ) and DI water as precursors in a typical cycle described as follows: 0.2 s pulse of DEZ, 40 s exposure, and 60 s purge with argon, followed by 2 s pulse of H_2O, 40 s exposure, and 60 s purge with argon.

Subsequently, electrodeposition of ZnO was performed using a previously reported procedure [37]. A three-electrode configuration was used with the ITO/PS spheres/ZnO ensemble as a working electrode, a Pt plate as the counter electrode, and Ag/AgCl as the reference electrode. An aqueous

solution of 0.05 mM $ZnCl_2$ (zinc precursor) and 0.1 M KCl (supporting electrolyte) was used as the electrolyte and was continuously bubbled with O_2 during the whole electrodeposition process. The electrodeposition was carried out at 80°C with a constant electric potential of -1 V during 15 min in a VersaSTAT 3 potentiostat. Once the electrodeposition was completed, the PS spheres were burned off in air at 600°C for 2 h. Finally, an Au layer (10, 30 and 50 nm) was deposited by a 350 UNIVEX e-beam evaporation system (10 kV, $1x10^{-6}$ mbar) on top of the substrates. The deposition thickness of Au was monitored using a quartz crystal monitor (deposition rate = 3 Å/s).

2.3 Substrate preparation for SERS measurements

To evaluate the enhancing capabilities of the substrates, thiophenol was selected as the test molecule. The substrates were immersed in a freshly prepared ethanolic solution with different concentrations (10^{-3} M – 10^{-8} M) of thiophenol for 18 h. After, the substrates were washed with copious amounts of anhydrous ethanol and dried in air under ambient conditions. For adenine detection, the substrates were immersed in different concentrations of adenine in DI water for 30 min. The substrates were then removed from the adenine solution and rinsed thoroughly with DI water and dried in air under ambient conditions.

2.4 Structural, SERS and extinction characterizations

The morphology of the as-prepared Au-covered urchin-like ZnO samples was characterized by a Hitachi S4800 scanning electron microscope (SEM). In addition, samples were prepared for Transmission electron (TEM) experiments by performing angular cuts using Focus Ion Beam (FIB) JEOL JIB-4000 using a gallium source working at 10 kV, with 60°, 40° and 30° incident angle geometries over a large area (50 μm). In this way, several particles were cut at different axis and geometry. TEM experiments were performed in an HR-TEM JEOL ARM-200F, working at 200kV, equipped with an energy-dispersive X-ray (EDX) detector. Samples were cut by FIB and then were sonicated in ethanol after ion milling and drop cast on commercially available Cu grids and vacuum dried overnight in a desiccator. X-Ray diffraction (XRD) was performed with a PANalytical X'pert-PRO diffractometer equipped with an X'celerator detector using Ni-filtered Cu Kα radiation. The XRD spectra were measured in the 2θ angular region between 20° and 70° with a scan speed of 2° min^{-1} and a step rate of roughly 0.02°/s. SERS measurements were performed with a Renishaw Invia Raman microscope with laser beams at 633 nm and 785 nm. The beam was focused with a 100 × objective lens with a N.A. = 0.9 in a backscattering geometry. The samples were irradiated with laser powers of 0.48 mW (633 nm) and 0.55 mW (785 nm) with acquisition times between 1 s and 10 s. For comparison, all the collected spectra were normalized by laser power and acquisition time. The average SERS intensities reported and relative standard deviations (RSD) were calculated with 25 SERS spectra. Moreover, a LabRam spectrophotometer is employed for the Raman measurements in solution (non-SERS reference) by using the same excitation wavelength and a macro-objective with a focal length of 40 mm (N.A. = 0.18). In addition, extinction spectra of samples were recorded in normal transmission mode with a Cary-5000 spectrophotometer from Agilent.

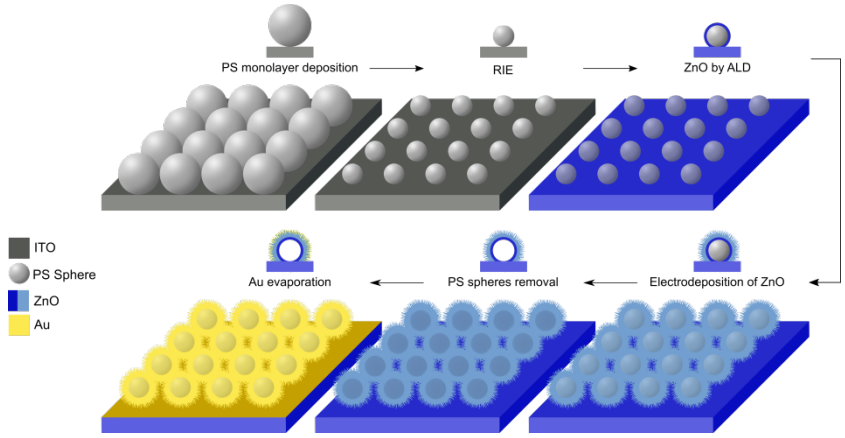

Figure 1. Scheme of the overall fabrication process

3. Results and discussion

The overall process for the fabrication of the Au-covered hollow urchin-like ZnO structures is depicted schematically in Fig. 1. Among the different approaches to fabricate ordered arrays of PS spheres, the direct assembly at the air-water interface has been demonstrated to be a simple and low-cost method that offers high-quality monolayers over large areas. Fig. 2a shows a SEM micrograph of a large area monolayer of PS spheres with a high degree of order. In order to produce a non-closed-packed monolayer, the PS spheres are exposed to oxygen plasma (Fig. 2b). This treatment allows controlling the size of the urchins and space between them. After reducing the size of the PS spheres, a thin 20-nm ZnO layer was deposited by ALD as a seed layer to promote the growth of ZnO NWs (Fig 2b). Owing to its high conformality and homogeneity, the ALD method promotes the uniform generation of ZnO NWs on the surface of the PS spheres, unlike pure hydrothermal methods or sputtering were the thickness control of the seed layer becomes a challenge [38]. In addition, the ALD layer anchors the PS spheres to the ITO substrate and renders their surface electrically conductive for the electrodeposition process. Fig. 2c shows the morphology of the urchin-like ZnO structures. Thanks to the homogenous ALD seed layer, the electrodeposited ZnO NWs are evenly distributed on the surface of the PS spheres. The size and length of the ZnO NWs of the urchin-like structures deposited by electrodeposition can be tuned by changing the electrochemical conditions (i.e., zinc precursor concentration and charge density) [39]. Finally, the urchins are homogenously covered by an Au film deposited via e-beam evaporation with thicknesses of 10, 30, and 50 nm, respectively. Fig. 2d shows the as-synthesized Au-covered urchin-like structures with a gold layer thickness of 30 nm (10 nm and 50 nm are shown on Fig. S1).

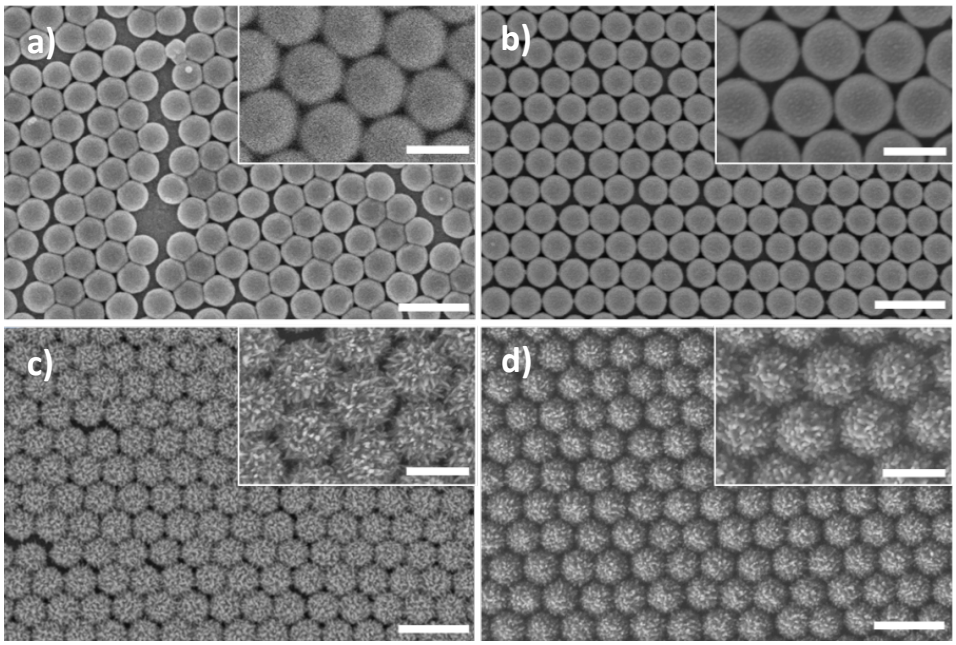

Figure 2. SEM micrographs of (a) an array of well-organized PS spheres, (b) PS spheres after been subjected to an oxygen plasma treatment, (c) ordered hollow urchin-like ZnO structures, and (d) urchin-like ZnO structures covered by a 30 nm-thick Au layer deposited by e-gun evaporation (scale bar = 1 μm). The insets show higher magnifications of the corresponding SEM images (scale bar = 500 nm).

The morphology and crystallinity of the urchin-like structures were studied by TEM. Fig. 3a clearly shows the Au film that covers the top of the urchin-like structures and the 20 nm ZnO seed film deposited by ALD. Notably, the TEM images display a cavity with a reduced contrast and a shell with a uniform dark gray color (Fig. S2), clearly showing the hollow character of the structures. The high-resolution (HR) TEM image from Fig. 3b shows the lattice fringes that correspond to ZnO and Au. Likewise, the FFT of the HRTEM image shows the (002) plane of ZnO. Additionally, to further confirm that the PS core of the urchin structures is removed after annealing, an EDX mapping was performed. Fig. 3c shows a scanning TEM (STEM) image of a single urchin structure and Fig. 3d shows the corresponding EDX elemental mapping of Fig. 3c. Fig. 3d shows that Zn and O are located in the core of the urchin, while Au is covering the outer shell of the structure.

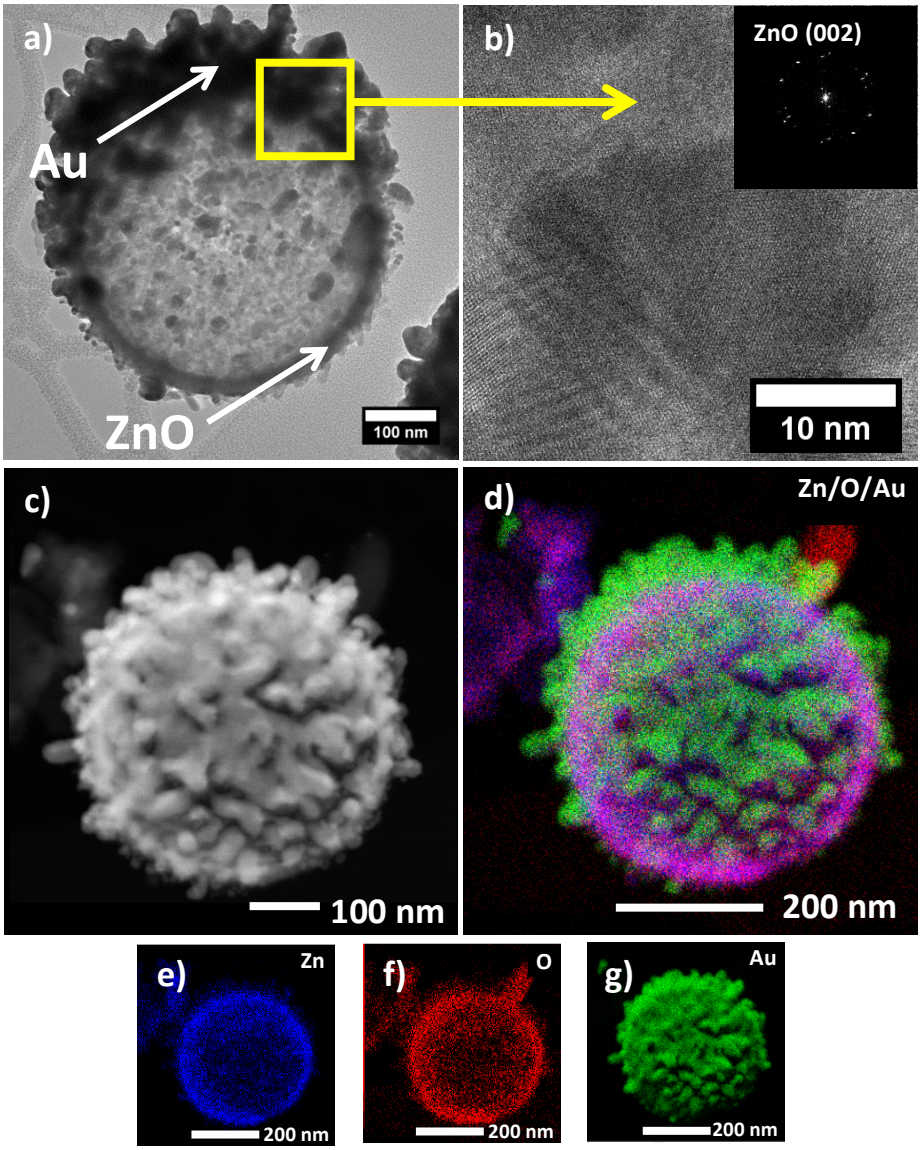

Figure 3. a) TEM image of an Au-covered ZnO urchin-like structure and b) high-resolution image of the selected area in image a). The inset in b) shows the FFT operation of the image. c) STEM and (d-g) EDX elemental mapping images of an Au-covered hollow ZnO urchin-like structure. Blue, red, and green illustrate Zn, O, and Au, respectively.

XRD measurements were carried out to study the crystallinity of the samples. The XRD patterns of ITO, urchin-like ZnO, and Au-covered urchin-like ZnO structures are displayed in Fig. S3. The diffraction peaks at 31.8°, 34.4°, and 36.4° can be assigned to the hexagonal würtzite planes of (100), (002), and (101) of ZnO [40,41], while the peaks at 38.2°, 44.5°, and 64.6° can be assigned to the face-centered-cubic (fcc) planes of (111), (200), and (220) of Au [42,43]. These results show the crystalline nature of the samples and the successful fabrication of a ZnO/Au composite. The remaining peaks correspond to the ITO film deposited on quartz that is used as a substrate [44].

3.1 SERS performances for chemical sensing

The SERS activity of the substrates was optimized by depositing different Au thicknesses. Fig. 4 shows the SERS spectra of thiophenol molecules grafted on the ZnO urchin-like structures covered with 10,

30, and 50 nm of gold for the two excitation wavelengths used here. Thiophenol was selected due to its ability to form self-assembled monolayers (SAMs) via S-Au bonds [45] and the absence of molecular vibrational activity near the selected excitation wavelengths (633 nm and 785 nm). The characteristic vibrational modes of thiophenol molecules (10^{-3} M) are well-observed (see refs [46-48]) like those at 999 cm^{-1} corresponding to the ring out-of-plane deformation and the C-H out-of-plane bending (noted, respectively: r-o-d and γ(CH)), 1022 cm^{-1} corresponding to the C-C symmetric stretching and the ring in-plane deformation (noted, respectively: ν(CC) and r-i-d), 1072 cm^{-1} corresponding to the C-C symmetric stretching and C-S stretching (noted, respectively: ν(CC) and ν(CS)), and at 1572 cm^{-1} the C-C symmetric stretching (noted: ν(CC)). For comparison, we studied the peak intensity at 999 cm^{-1}. It is noticeable that the Raman peaks intensities become larger as we increase the Au layer thickness for the two excitation wavelengths. This is in accordance with literature reports where it is shown that the thickness of the metallic layer plays an important role on the overall SERS enhancement [49–51]. For our complete study, we chose the 30-nm thickness with the excitation wavelength of 785 nm in order to obtain a good compromise between the SERS signal enhancement and a low overall cost of production of these SERS substrates. Fig. 5a shows the thiophenol spectra obtained from different structures for the purpose of comparison. When ZnO nanowires covered with Au (30 nm) of a size comparable from those on the ZnO urchin-like structures are used, the characteristic Raman peaks of thiophenol can barely be distinguished. Similarly, for the bare Au film (30 nm), the thiophenol peaks can be hardly identified. This result shows that the urchin-like structures present the highest SERS activity from these three types of substrate configurations.

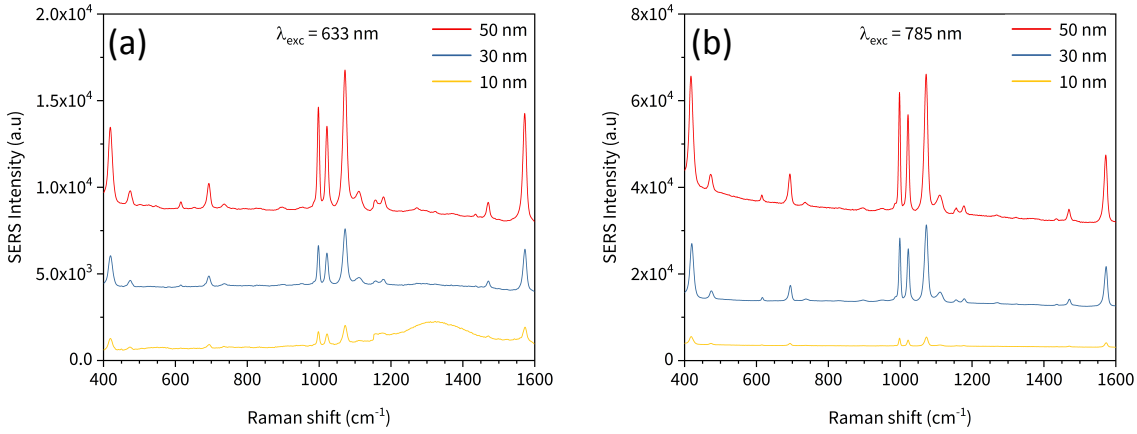

Figure 4. SERS spectra of thiophenol (10^{-3} M) from different Au film thicknesses (10, 30, and 50 nm) for the two excitation wavelengths used in our experiments: (a) 633 nm and (b) 785 nm.

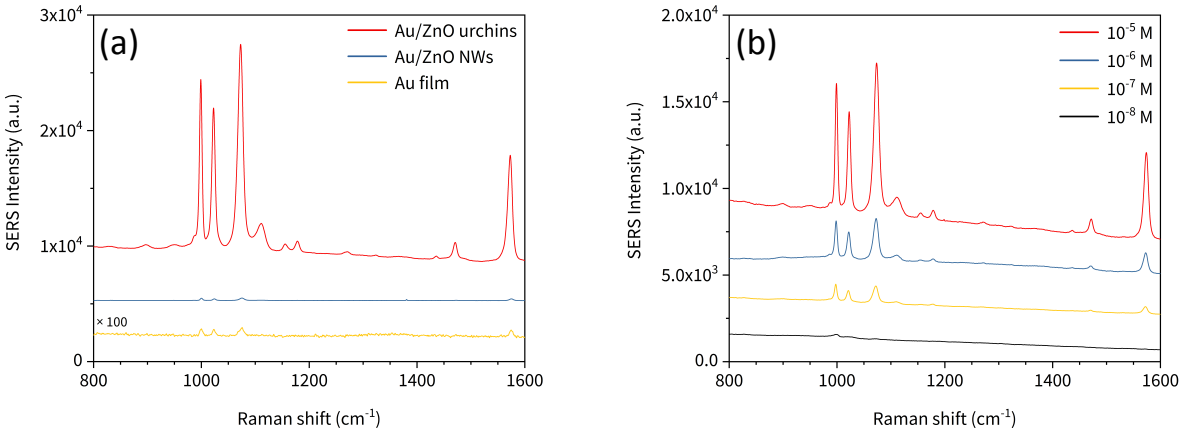

Figure 5. (a) SERS spectra of thiophenol (10^{-3} M) from a 30-nm Au film, a 30-nm Au ZnO NWs, and a 30-nm Au covered urchin-like ZnO, which present an offset to improve the data visualization. (b) SERS spectra of the 30 nm Au-covered ZnO urchins with different thiophenol concentrations. The spectra are not background-corrected, and recorded at the excitation wavelength of 785 nm.

Given the complex 3D morphology of the urchins, it is difficult to know the exact number of molecules that are excited in the SERS measurements [52,53]. For this reason, the EF for the 30 nm Au-covered ZnO urchins SERS substrates was calculated by using the formula: EF ≈ I_{SERS}/I_{ref} [10] were I_{ref} represents the Raman intensity of a thiophenol solution in ethanol (1 M; see fig. S4 in SI) and I_{SERS} represents the Raman intensity of the SERS measurements. Thus, the highest EF value for the Raman peak at 1572 cm^{-1} was 5.3×10^2 (Table 1). From the extinction spectra (see figure 6), we observed that the excitation wavelengths of 633 nm and 785 nm are, respectively, more and more close to maximum of one resonance when the gold thickness increases that can significantly improve the enhancement factor. Moreover, it is known that EF is proportional to the extinction intensities (Q_e) [50,54], i.e. $EF \sim Q_e(\lambda_{exc}) \times Q_e(\lambda_{Raman})$. We observed that the EF values (see Table 1) follow qualitatively the same trend than those observed from the extinction spectra. These EF values can be attributed to the combination of different effects such as efficient light trapping [31] and the generation of hotspots from almost-touching NWs from adjacent urchins [55]. Additionally, the size of the gaps between the Au-covered urchin-like structures is in the same range as the excitation wavelength, which could contribute to the enhancement of localized electromagnetic fields and effective absorption of light by the LSPR [10,32]. SERS measurements with a range of molecular concentrations from 10^{-5} M – 10^{-8} M were performed in order to assess the limit of detection (LOD) of the substrates. Fig. 5b shows the Raman spectra of the substrates grafted with different thiophenol concentrations. The intensities of the Raman peaks remain strong up to a concentration of 10^{-7} M and then fall considerably for the concentration of 10^{-8} M where only the peak at 999 cm^{-1} remains visible. This LOD is comparable with values reported in the literature for thiophenol and similar Au-based structures [47,50].

Raman shift (cm^{-1})	999	1022	1072	1572
I_{SERS}	15066	12199	16926	9539
I_{Raman}	79	32	55	18
EF	1.9×10^2	3.8×10^2	3.1×10^2	5.3×10^2

Table 1. Calculated enhancement factors (EF) for four Raman peaks (1 mM of thiophenol) at the excitation wavelength of 785 nm for ZnO urchin-like structures covered with a 30-nm Au film.

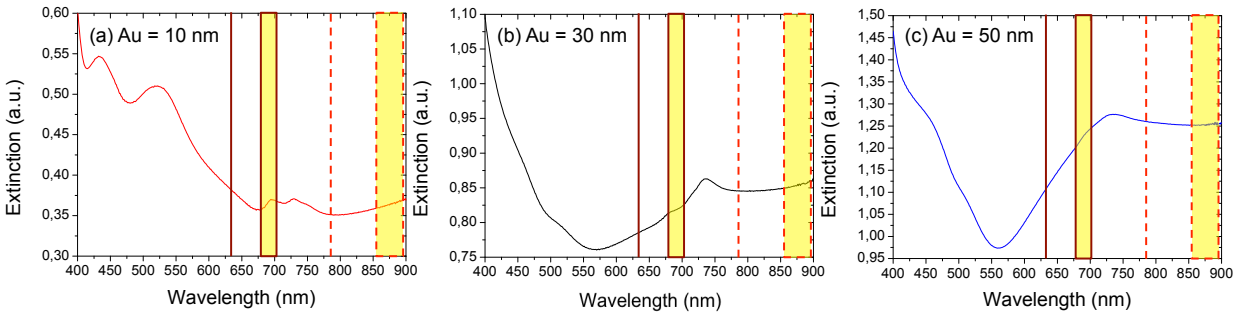

Figure 6. Extinction spectra of Au/ZnO-urchins with different thicknesses of gold: (a) Au = 10 nm, (b) Au = 30 nm, and (c) Au = 50 nm. On each extinction spectrum, the excitation wavelengths of 633 nm (dark red line) and 785 nm (red dashed line) are displayed, and also the region of the corresponding Raman scattering wavelengths (999 to 1572 cm^{-1}; dark red/yellow rectangle associated to the excitation wavelength of 633 nm, and dashed red/yellow rectangle those associated to the excitation wavelength of 785 nm).

3.2 Uniformity and substrate-to-substrate reproducibility of SERS signal

To demonstrate the large-area uniformity of the Au-covered hollow urchin-like structures, we constructed a Raman intensity map of the 999 cm^{-1} peak over a 20 × 20 μm^2 area with a step size of 1 μm (Fig. 7a). The 400-point map shows an almost continuous bright-colored area with a few darker spots where the intensity is lower, which demonstrates the reasonable uniformity of the substrate.

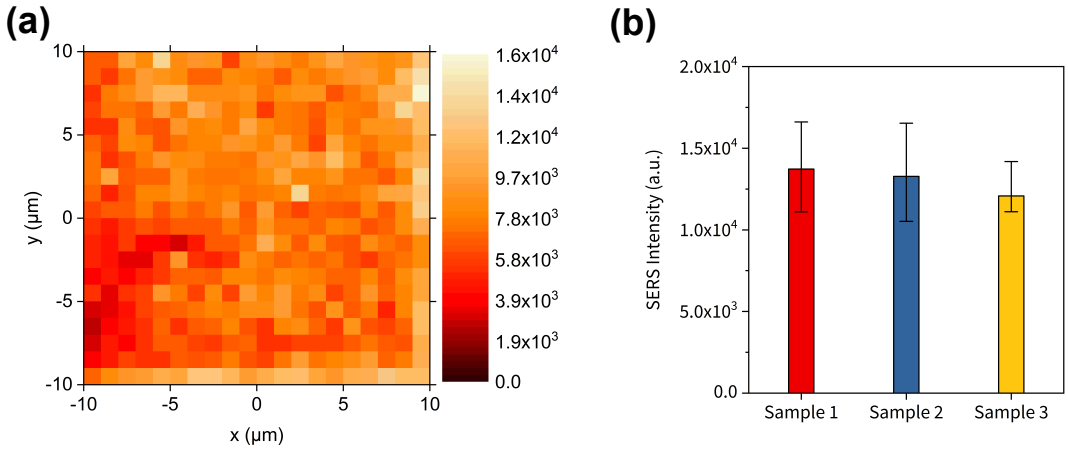

Figure 7. (a) Raman map image of the 999 cm^{-1} peak from a randomly selected area (20 x 20 μm^2) on the Au-covered hollow urchin-like structures at the 785-nm excitation wavelength. (b) Intensity distribution of the 999 cm^{-1} peak of three different samples with an average RSD value < 10%.

Additionally, the substrate-to-substrate reproducibility was investigated by measuring the intensity of the 999 cm^{-1} peak from three different batches. Fig. 7b shows the intensity distribution for three different samples. The average RSD value was found to be < 10%, which indicates a good reproducibility of the SERS substrates and shows their excellent performance.

3.2 SERS performances for biological sensing

Finally, to demonstrate the biosensing capability of these substrates, we chose the biomolecule adenine which can be used in the detection of DNA or RNA analytes [10,27]. Fig. 8 shows SERS spectra of Adenine at three different concentrations using the urchin-like ZnO structures covered with 30 nm of Au, and recorded at the excitation wavelength of 785 nm. The characteristic purine stretch at 736 cm^{-1} is noticeable up to a concentration of 1 μM and the spectra show a low signal-to-noise ratio, which is beneficial for future biosensing applications and is comparable to results published in the literature [10,27].

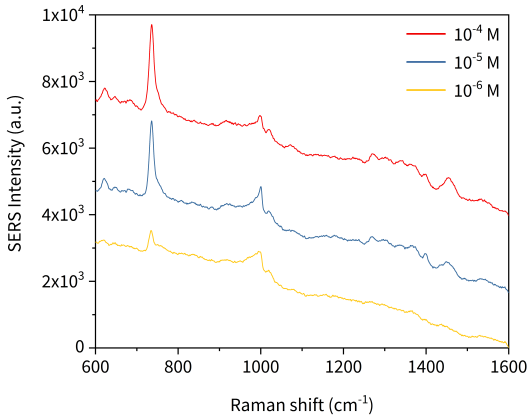

Figure 8. SERS spectra for different concentrations of adenine with a LOD of 1 μM.

4. Conclusion

In summary, high-surface-area Au-covered hollow ZnO urchin-like structures were prepared by combining NSL, ALD, electrodeposition, and e-beam evaporation. These high-throughput methods are readily scalable and allow the precise control of the size of the urchins and the interparticle distance. The amplification of the SERS signal for thiophenol was investigated by depositing different thicknesses of Au, and the 30-nm thickness was selected for its good compromise between the enhancement of the SERS intensity and the low cost of production. The LOD of the selected substrates was tested by detecting thiophenol down to 10^{-8} M. Additionally, the batch-to-batch repeatability was demonstrated and an average RSD < 10% was obtained. Finally, adenine was detected up to a concentration of 10^{-6} M in order to demonstrate the biosensing capability of our substrate. These results suggest that the Au-covered hollow urchin-like ZnO structures are viable candidates for ultrasensitive and reproducible SERS sensing and biosensing.

Acknowledgements

O.G. would like to thank CONACYT, México for funding. I.I. acknowledges the financial support from the National Science Centre of Poland by the SONATA 11 project UMO-2016/21/D/ST3/00962. We thank Sophie Tingry for use and assistance with the potentiostat used in this study. This work was supported by the European Union's Horizon 2020 research and innovation program "CanBioSe" (grant agreement no. 778157).

References

[1] K. Kneipp, Y. Wang, H. Kneipp, L.T. Perelman, I. Itzkan, R.R. Dasari, M.S. Feld, Single Molecule Detection Using Surface-Enhanced Raman Scattering (SERS), Phys. Rev. Lett. 78 (1997) 1667–1670. doi:10.1103/PhysRevLett.78.1667.

[2] J.Q. Xue, D.W. Li, L.L. Qu, Y.T. Long, Surface-imprinted core-shell Au nanoparticles for selective detection of bisphenol A based on surface-enhanced Raman scattering, Anal. Chim. Acta. 777 (2013) 57–62. doi:10.1016/j.aca.2013.03.037.

[3] L.A. Lane, X. Qian, S. Nie, SERS Nanoparticles in Medicine: From Label-Free Detection to Spectroscopic Tagging, Chem. Rev. 115 (2015) 10489–10529. doi:10.1021/acs.chemrev.5b00265.

[4] R.M. Jarvis, R. Goodacre, Characterisation and identification of bacteria using SERS, Chem. Soc. Rev. 37 (2008) 931. doi:10.1039/b705973f.

[5] R.A. Halvorson, P.J. Vikesland, Surface-enhanced Raman spectroscopy (SERS) for environmental analyses, Environ. Sci. Technol. 44 (2010) 7749–7755. doi:10.1021/es101228z.

[6] K.A. Willets, R.P. Van Duyne, Localized surface plasmon resonance spectroscopy and sensing, Annu. Rev. Phys. Chem. 58 (2007) 267–97. doi:10.1146/annurev.physchem.58.032806.104607.

[7] M. Bechelany, P. Brodard, L. Philippe, J. Michler, Extended domains of organized nanorings of silver grains as surface-enhanced Raman scattering sensors for molecular detection, Nanotechnology. 20 (2009) 455302. doi:10.1088/0957-4484/20/45/455302.

[8] J. Stropp, G. Trachta, G. Brehm, S. Schneider, A new version of AgFON substrates for high-throughput analytical SERS applications, J. Raman Spectrosc. 34 (2003) 26–32. doi:10.1002/jrs.931.

[9] Y. Li, J. Dykes, T. Gilliam, N. Chopra, A new heterostructured SERS substrate: free-standing silicon nanowires decorated with graphene-encapsulated gold nanoparticles, Nanoscale. 9 (2017) 5263–5272. doi:10.1039/C6NR09896G.

[10] H.M. Jin, J.Y. Kim, M. Heo, S.-J. Jeong, B.H. Kim, S.K. Cha, K.H. Han, J.H. Kim, G.G. Yang, J. Shin, S.O. Kim, Ultralarge Area Sub-10 nm Plasmonic Nanogap Array by Block Copolymer Self-Assembly for Reliable High-Sensitivity SERS, ACS Appl. Mater. Interfaces. 10 (2018) acsami.8b17325. doi:10.1021/acsami.8b17325.

[11] C. Cheng, B. Yan, S.M. Wong, X. Li, W. Zhou, T. Yu, Z. Shen, H. Yu, H.J. Fan, Fabrication and SERS Performance of Silver-Nanoparticle-Decorated Si/ZnO Nanotrees in Ordered Arrays, ACS Appl. Mater. Interfaces. 2 (2010) 1824–1828. doi:10.1021/am100270b.

[12] W. Kim, S.H. Lee, S.H. Kim, J.-C. Lee, S.W. Moon, J.S. Yu, S. Choi, Highly Reproducible Au-Decorated ZnO Nanorod Array on a Graphite Sensor for Classification of Human Aqueous Humors, ACS Appl. Mater. Interfaces. 9 (2017) 5891–5899. doi:10.1021/acsami.6b16130.

[13] S.M. Asiala, Z.D. Schultz, Characterization of hotspots in a highly enhancing SERS substrate, Analyst. 136 (2011) 4472. doi:10.1039/c1an15432j.

[14] I. Alessandri, J.R. Lombardi, Enhanced Raman Scattering with Dielectrics, Chem. Rev. 116 (2016) 14921–14981. doi:10.1021/acs.chemrev.6b00365.

[15] M. Nasr, C. Eid, R. Habchi, P. Miele, M. Bechelany, Recent Progress on Titanium Dioxide Nanomaterials for Photocatalytic Applications, ChemSusChem. 11 (2018) 3023–3047. doi:10.1002/cssc.201800874.

[16] X. Zhang, Y. Liu, Z. Kang, 3D Branched ZnO Nanowire Arrays Decorated with Plasmonic Au Nanoparticles for High-Performance Photoelectrochemical Water Splitting, ACS Appl. Mater. Interfaces. 6 (2014) 4480–4489. doi:10.1021/am500234v.

[17] C. Karam, C. Guerra-Nuñez, R. Habchi, Z. Herro, N. Abboud, A. Khoury, S. Tingry, P. Miele, I. Utke, M. Bechelany, Urchin-inspired ZnO-TiO_2core-shell as building blocks for dye sensitized solar cells, Mater. Des. 126 (2017) 314–321. doi:10.1016/j.matdes.2017.04.019.

[18] O. Graniel, M. Weber, S. Balme, P. Miele, M. Bechelany, Atomic layer deposition for biosensing applications, Biosens. Bioelectron. 122 (2018) 147–159. doi:10.1016/j.bios.2018.09.038.

[19] O. Graniel, V. Fedorenko, R. Viter, I. Iatsunskyi, G. Nowaczyk, M. Weber, K. Załęski, S. Jurga, V. Smyntyna, P. Miele, A. Ramanavicius, S. Balme, M. Bechelany, Optical properties of ZnO deposited by atomic layer deposition (ALD) on Si nanowires, Mater. Sci. Eng. B. 236–237 (2018) 139–146. doi:10.1016/j.mseb.2018.11.007.

[20] I. Iatsunskyi, A. Vasylenko, R. Viter, M. Kempiński, G. Nowaczyk, S. Jurga, M. Bechelany, Tailoring of the electronic properties of ZnO-polyacrylonitrile nanofibers: Experiment and theory, Appl. Surf. Sci. 411 (2017) 494–501. doi:10.1016/j.apsusc.2017.03.111.

[21] L. Yang, Y. Yang, Y. Ma, S. Li, Y. Wei, Z. Huang, N. Long, Fabrication of Semiconductor ZnO Nanostructures for Versatile SERS Application, Nanomaterials. 7 (2017) 398. doi:10.3390/nano7110398.

[22] K.C. Bantz, A.F. Meyer, N.J. Wittenberg, H. Im, Ö. Kurtuluş, S.H. Lee, N.C. Lindquist, S.-H. Oh, C.L. Haynes, Recent progress in SERS biosensing, Phys. Chem. Chem. Phys. 13 (2011) 11551. doi:10.1039/c0cp01841d.

[23] J.C. Hulteen, R.P. Van Duyne, Nanosphere lithography: A materials general fabrication process for periodic particle array surfaces, J. Vac. Sci. Technol. A Vacuum, Surfaces, Film. 13 (1995) 1553. doi:10.1116/1.579726.

[24] S. Sakamoto, L. Philippe, M. Bechelany, J. Michler, H. Asoh, S. Ono, Ordered hexagonal array of Au nanodots on Si substrate based on colloidal crystal templating, Nanotechnology. 19 (2008) 405304. doi:10.1088/0957-4484/19/40/405304.

[25] J. Lee, Q. Zhang, S. Park, A. Choe, Z. Fan, H. Ko, Particle–Film Plasmons on Periodic Silver Film over Nanosphere (AgFON): A Hybrid Plasmonic Nanoarchitecture for Surface-Enhanced Raman Spectroscopy, ACS Appl. Mater. Interfaces. 8 (2016) 634–642. doi:10.1021/acsami.5b09753.

[26] X. Li, H. Hu, D. Li, Z. Shen, Q. Xiong, S. Li, H.J. Fan, Ordered Array of Gold Semishells on TiO_2 Spheres: An Ultrasensitive and Recyclable SERS Substrate, ACS Appl. Mater. Interfaces. 4 (2012) 2180–2185. doi:10.1021/am300189n.

[27] H. Im, K.C. Bantz, S.H. Lee, T.W. Johnson, C.L. Haynes, S.-H. Oh, Self-Assembled Plasmonic Nanoring Cavity Arrays for SERS and LSPR Biosensing, Adv. Mater. 25 (2013) 2678–2685. doi:10.1002/adma.201204283.

[28] M. Tabatabaei, A. Sangar, N. Kazemi-Zanjani, P. Torchio, A. Merlen, F. Lagugné-Labarthet, Optical properties of silver and gold tetrahedral nanopyramid arrays prepared by nanosphere lithography, J. Phys. Chem. C. 117 (2013) 14778–14786. doi:10.1021/jp405125c.

[29] G. Quero, G. Zito, S. Managò, F. Galeotti, M. Pisco, A. De Luca, A. Cusano, Nanosphere Lithography on Fiber: Towards Engineered Lab-On-Fiber SERS Optrodes, Sensors. 18 (2018) 680. doi:10.3390/s18030680.

[30] X. He, C. Yue, Y. Zang, J. Yin, S. Sun, J. Li, J. Kang, Multi-hot spot configuration on urchin-like Ag nanoparticle/ZnO hollow nanosphere arrays for highly sensitive SERS, J. Mater. Chem. A. 1 (2013) 15010–15015. doi:10.1039/c3ta13450d.

[31] Q. Tao, S. Li, C. Ma, K. Liu, Q.-Y. Zhang, A highly sensitive and recyclable SERS substrate based on Ag-nanoparticle-decorated ZnO nanoflowers in ordered arrays, Dalt. Trans. 44 (2015) 3447–3453. doi:10.1039/C4DT03596H.

[32] R. Li, C. Han, Q.W. Chen, A facile synthesis of multifunctional ZnO/Ag sea urchin-like hybrids as highly sensitive substrates for surface-enhanced Raman detection, RSC Adv. 3 (2013) 11715–11722. doi:10.1039/c3ra41203b.

[33] M. Erol, Y. Han, S.K. Stanley, C.M. Stafford, H. Du, S. Sukhishvili, SERS not to be taken for granted in the presence of oxygen, J. Am. Chem. Soc. 131 (2009) 7480–7481. doi:10.1021/ja807458x.

[34] Y. Han, R. Lupitskyy, T.M. Chou, C.M. Stafford, H. Du, S. Sukhishvili, Effect of oxidation on surface-enhanced raman scattering activity of silver nanoparticles: A quantitative correlation, Anal. Chem. 83 (2011) 5873–5880. doi:10.1021/ac2005839.

[35] M. Weber, A. Julbe, A. Ayral, P. Miele, M. Bechelany, Atomic Layer Deposition for Membranes: Basics, Challenges, and Opportunities, Chem. Mater. 30 (2018) 7368–7390. doi:10.1021/acs.chemmater.8b02687.

[36] N. Vogel, S. Goerres, K. Landfester, C.K. Weiss, A convenient method to produce close- and non-close-packed monolayers using direct assembly at the air-water interface and subsequent plasma-induced size reduction, Macromol. Chem. Phys. 212 (2011) 1719–1734. doi:10.1002/macp.201100187.

[37] J. Elias, C. Léuy-Clément, M. Bechelany, J. Michler, G.Y. Wang, Z. Wang, L. Philippe, Hollow urchin-like ZnO thin films by electrochemical deposition, Adv. Mater. 22 (2010) 1607–1612. doi:10.1002/adma.200903098.

[38] G. Sinha, L.E. Depero, I. Alessandri, Recyclable SERS Substrates Based on Au-Coated ZnO Nanorods, ACS Appl. Mater. Interfaces. 3 (2011) 2557–2563. doi:10.1021/am200396n.

[39] J. Elias, M. Bechelany, I. Utke, R. Erni, D. Hosseini, J. Michler, L. Philippe, Urchin-inspired zinc oxide as building blocks for nanostructured solar cells, Nano Energy. 1 (2012) 696–705. doi:10.1016/j.nanoen.2012.07.002.

[40] A.A. Chaaya, R. Viter, I. Baleviciute, M. Bechelany, A. Ramanavicius, Z. Gertnere, D. Erts, V. Smyntyna, P. Miele, Tuning Optical Properties of Al2O3/ZnO Nanolaminates Synthesized by Atomic Layer Deposition, J. Phys. Chem. C. 118 (2014) 3811–3819. doi:10.1021/jp411970w.

[41] A. Di Mauro, M. Cantarella, G. Nicotra, V. Privitera, G. Impellizzeri, Low temperature atomic layer deposition of ZnO: Applications in photocatalysis, Appl. Catal. B Environ. 196 (2016) 68–76. doi:10.1016/j.apcatb.2016.05.015.

[42] R. Viter, Z. Balevicius, A. Abou Chaaya, I. Baleviciute, S. Tumenas, L. Mikoliunaite, A. Ramanavicius, Z. Gertnere, A. Zalesska, V. Vataman, V. Smyntyna, D. Erts, P. Miele, M. Bechelany, The influence of localized plasmons on the optical properties of Au/ZnO nanostructures, J. Mater. Chem. C. 3 (2015) 6815–6821. doi:10.1039/C5TC00964B.

[43] S. Arunkumar, T. Hou, Y.-B. Kim, B. Choi, S.H. Park, S. Jung, D.-W. Lee, Au Decorated ZnO hierarchical architectures: Facile synthesis, tunable morphology and enhanced CO detection at room temperature, Sensors Actuators B Chem. 243 (2017) 990–1001. doi:10.1016/j.snb.2016.11.152.

[44] Z. Ghorannevis, E. Akbarnejad, M. Ghoranneviss, Structural and morphological properties of ITO thin films grown by magnetron sputtering, J. Theor. Appl. Phys. 9 (2015) 285–290. doi:10.1007/s40094-015-0187-3.

[45] B.-S. Lee, D.-Z. Lin, T.-J. Yen, A Low-cost, Highly-stable Surface Enhanced Raman Scattering Substrate by Si Nanowire Arrays Decorated with Au Nanoparticles and Au Backplate, Sci. Rep. 7 (2017) 4604. doi:10.1038/s41598-017-04062-4.

[46] S. Li, D. Wu, X. Xu, R. Gu, Theoretical and experimental studies on the adsorption behavior of thiophenol on gold nanoparticles, J. Raman Spectrosc. 38 (2007) 1436–1443. doi:10.1002/jrs.1791.

[47] L. Scarabelli, M. Coronado-Puchau, J.J. Giner-Casares, J. Langer, L.M. Liz-Marzán, Monodisperse Gold Nanotriangles: Size Control, Large-Scale Self-Assembly, and Performance in Surface-Enhanced Raman Scattering, ACS Nano. 8 (2014) 5833–5842. doi:10.1021/nn500727w.

[48] J.-F. Bryche, A. Tsigara, B. Bélier, M. Lamy de la Chapelle, M. Canva, B. Bartenlian, G. Barbillon, Surface enhanced Raman scattering improvement of gold triangular nanoprisms by a gold reflective underlayer for chemical sensing, Sensors Actuators B Chem. 228 (2016) 31–35. doi:10.1016/j.snb.2016.01.018.

[49] C. Lee, C.S. Robertson, A.H. Nguyen, M. Kahraman, S. Wachsmann-Hogiu, Thickness of a metallic film, in addition to its roughness, plays a significant role in SERS activity, Sci. Rep. 5 (2015) 11644. doi:10.1038/srep11644.

[50] G. Magno, B. Bélier, G. Barbillon, Gold thickness impact on the enhancement of SERS detection in low-cost Au/Si nanosensors, J. Mater. Sci. 52 (2017) 13650–13656. doi:10.1007/s10853-017-1445-3.

[51] H. Schneidewind, K. Weber, M. Zeisberger, U. Hübner, A. Dellith, D. Cialla-May, R. Mattheis, J. Popp, The effect of silver thickness on the enhancement of polymer based SERS substrates, Nanotechnology. 25 (2014) 445203. doi:10.1088/0957-4484/25/44/445203.

[52] E.C. Le Ru, E.J. Blackie, M. Meyer, P.G. Etchegoin, Surface Enhanced Raman Scattering Enhancement Factors: A Comprehensive Study, J. Phys. Chem. C. 111 (2007) 13794–13803. doi:10.1021/jp0687908.

[53] G. Barbillon, V.E. Sandana, C. Humbert, B. Bélier, D.J. Rogers, F.H. Teherani, P. Bove, R. McClintock, M. Razeghi, Study of Au coated ZnO nanoarrays for surface enhanced Raman scattering chemical sensing, J. Mater. Chem. C. 5 (2017) 3528–3535. doi:10.1039/C7TC00098G.

[54] P.G. Etchegoin, E.C. Le Ru, Basic Electromagnetic Theory of SERS. In *Surface Enhanced Raman Spectroscopy: Analytical, Biophysical and Life Science Applications*; S. Schlücker, Ed.; Wiley-VCH: Weinheim, Germany, 2011; pp. 1-34, ISBN 978-3-527-32567-2.

[55] Z. Li, K. Sun, Z. Du, B. Chen, X. He, Galvanic-Cell-Reaction-Driven Deposition of Large-Area Au Nanourchin Arrays for Surface-Enhanced Raman Scattering., Nanomaterials. 8 (2018) 265. doi:10.3390/nano8040265.